J Biomol NMR
DOI 10.1007/s10858-010-9416-x

ARTICLE

Tunable paramagnetic relaxation enhancements by $[Gd(DPA)_3]^{3-}$ for protein structure analysis

Hiromasa Yagi · Karin V. Loscha · Xun-Cheng Su · Mitchell Stanton-Cook · Thomas Huber · Gottfried Otting

Received: 22 February 2010 / Accepted: 26 March 2010

Abstract Paramagnetic relaxation enhancements (PRE) present a powerful source of structural information in nuclear magnetic resonance (NMR) studies of proteins and protein–ligand complexes. In contrast to conventional PRE reagents that are covalently attached to the protein, the complex between gadolinium and three dipicolinic acid (DPA) molecules, $[Gd(DPA)_3]^{3-}$, can bind to proteins in a non-covalent yet site-specific manner. This offers straightforward access to PREs that can be scaled by using different ratios of $[Gd(DPA)_3]^{3-}$ to protein, allowing quantitative distance measurements for nuclear spins within about 15 Å of the Gd^{3+} ion. Such data accurately define the metal position relative to the protein, greatly enhancing the interpretation of pseudocontact shifts induced by $[Ln(DPA)_3]^{3-}$ complexes of paramagnetic lanthanide (Ln^{3+}) ions other than gadolinium. As an example we studied the quaternary structure of the homodimeric GCN4 leucine zipper.

Keywords Lanthanide tags · Leucine zipper · NMR spectroscopy · Paramagnetic relaxation enhancements · Pseudocontact shifts

Electronic supplementary material The online version of this article (doi:10.1007/s10858-010-9416-x) contains supplementary material, which is available to authorized users.

H. Yagi · K. V. Loscha · X.-C. Su · G. Otting (✉)
Research School of Chemistry, Australian National University, Canberra, ACT 0200, Australia
e-mail: gottfried.otting@anu.edu.au

M. Stanton-Cook · T. Huber
School of Chemistry and Molecular Biosciences, University of Queensland, Brisbane, QLD 4072, Australia

Introduction

Paramagnetic tags have become a widely used source of structural information in studies of proteins and macromolecular interactions by NMR spectroscopy (for recent reviews see, e.g., Clore and Iwahara 2009; Su and Otting 2010). Paramagnetic centers can be made of stable organic radicals or paramagnetic metal ions. Nitroxide radicals, Mn^{2+}, and Gd^{3+} ions stand out for their long electronic relaxation times which lead to paramagnetic relaxation enhancements (PRE) by a dipole–dipole mechanism that decreases as r^{-6} with increasing distance r between the paramagnetic center and the nuclear spin (Solomon 1955; Bloembergen and Morgan 1961). PREs from other metal ions are more problematic because metal ions with rapidly relaxing unpaired electron spins change the chemical shifts. In addition, they relax nuclear spins by the Curie relaxation mechanism (Guéron 1975; Vega and Fiat 1976) and cross-correlation effects between nuclear relaxation due to chemical shift anisotropy and Curie relaxation compromise the usual r^{-6} distance dependence of PRE (Pintacuda et al. 2004a). In contrast, PREs from nitroxides, Mn^{2+}, and Gd^{3+} are readily interpreted by a r^{-6} distance dependence. Unlike other paramagnetic metals, these probes also preserve the chemical shifts in the NMR spectrum.

Nitroxides, Mn^{2+}, and Gd^{3+} ions are highly paramagnetic and the resulting PREs cause excessive line broadening of NMR signals of nuclear spins close to the paramagnetic center. This makes it difficult to explore structural features in the vicinity of one of these paramagnetic probes if it is covalently attached to the molecule of interest. Here we present an alternative approach, using a Gd^{3+} complex that binds non-covalently yet site-specifically to measure PRE effects quantitatively near the paramagnetic center.

Published online: 20 April 2010

We recently showed that the 3:1 complex between dipicolinic acid (DPA) and lanthanide ions (Ln^{3+}), $[Ln(DPA)_3]^{3-}$, binds site-specifically to a number of proteins with dissociation constants K_D ranging from tens of micromoles to millimoles (Su et al. 2009). For all proteins studied to date, the $[Ln(DPA)_3]^{3-}$ complexes are in fast exchange between the bound and free states (Su et al. 2009). Using $[Gd(DPA)_3]^{3-}$, the magnitude of the PRE effect can thus be tuned simply by the ratio of Gd^{3+} complex to protein. This allows PRE measurements over a wide distance range, starting from nuclear spins in the vicinity of the paramagnetic ion. In addition, using the structure coordinates of the binding site, PREs of nuclear spins near the metal can be used for accurate determination of the metal position. The lanthanide coordinates determined using $[Gd(DPA)_3]^{3-}$ can subsequently be used to assist in the interpretation of pseudocontact shifts (PCS) induced by $[Ln(DPA)_3]^{3-}$ complexes with paramagnetic lanthanides other than Gd^{3+}.

PCSs contain unique long-range structural information with outstanding potential for 3D structure determinations of proteins and protein–protein and protein–ligand complexes (Arnesano et al. 2005; Balayssac et al. 2008; Bertini et al. 2008; Otting 2008; Pintacuda et al. 2007; Ubbink 2009). PCSs depend on the polar coordinates r, θ, and ϕ of the nuclear spin with respect to the principal axes of the magnetic susceptibility anisotropy ($\Delta\chi$) tensor of the metal ion and the axial and rhombic components of the $\Delta\chi$ tensor

$$\Delta\delta^{PCS} = 1/(12\pi r^3)[\Delta\chi_{ax}(3\cos^2\theta - 1) + 1.5\Delta\chi_{rh}\sin^2\theta\ \cos 2\phi] \quad (1)$$

where $\Delta\delta^{PCS}$ denotes the pseudocontact shift measured in ppm. Interpretation of PCSs thus requires fitting of the eight parameters of the $\Delta\chi$ tensor ($\Delta\chi_{ax}$, $\Delta\chi_{rh}$, three Euler angles relating the $\Delta\chi$ tensor to the molecular frame and the x, y, z coordinates of the metal ion) to the molecular coordinates. Prior determination of the metal coordinates using PREs reduces the fit to five parameters.

The present work used the GCN4 leucine zipper as a model system. GCN4 is a transcriptional regulator with a dimeric leucine zipper in the last 33 residues of the protein. The leucine zipper forms a highly stable (O'Shea et al. 1989; Matousek et al. 2007) two-stranded, parallel coiled coil (O'Shea et al. 1991). NMR data show only a single set of resonances for both monomers, indicating that the dimer is symmetric in the time average (Oas et al. 1990; O'Donoghue et al. 1996). Establishing the packing mode of coiled-coil proteins by NMR spectroscopy requires unconventional means (O'Donoghue et al. 1996; Zweckstetter et al. 2005).

In the following we show that $[Gd(DPA)_3]^{3-}$ binds site-specifically to the GCN4 leucine zipper, use the PREs to locate the lanthanide ion, determine the $\Delta\chi$ tensors of different $[Ln(DPA)_3]^{3-}$ complexes bound to the peptide, and use the PCSs to assess the quaternary structure of the peptide. In addition, intermolecular PREs from non-specifically binding $[Gd(DPA)_3]^{3-}$ are compared to those from the established Gd(DTPA-BMA) probe (Pintacuda and Otting 2002).

Materials and methods

Uniformly ^{15}N-labeled GCN4 leucine zipper was expressed and purified as a C-terminal fusion with His_6-tagged ubiquitin followed by cleavage with His-tagged deubiquitinating enzyme (Baker et al. 2005) to yield the authentic amino terminus. Details are described in the Supporting Information. The amino acid sequence of the resulting 33 residue peptide was RMKQLEDKVEELLSKNYHLENEVARLKKLVGER.

NMR spectra were recorded using 0.3 or 1.5 mM (monomer) solutions of leucine zipper in 20 mM MES buffer, pH 6.0, at 25°C on Bruker Avance 600 and 800 MHz NMR spectrometers equipped with TCI cryoprobes. The backbone amide resonances were assigned using a 3D NOESY-^{15}N-HSQC spectrum.

The binding affinity of $[Ln(DPA)_3]^{3-}$ to the GCN4 peptide was measured by monitoring the ^1H chemical shifts of ^{15}N-HSQC cross peaks with increasing concentrations of the $[Yb(DPA)_3]^{3-}$ complex. The K_D value was fitted using a 1:1 binding model.

All relaxation measurements were performed at a ^1H NMR frequency of 800 MHz. Transverse ^1H relaxation rates were measured by two time point (0 and 13.5 ms) measurements (Iwahara et al. 2007). Longitudinal ^1H relaxation rates were measured by preceding the ^{15}N-HSQC pulse sequence by a 180°(^1H) pulse and a relaxation delay (inversion-recovery; Vold et al. 1968). Transverse and longitudinal PREs (Γ_2 and Γ_1, respectively) induced by $[Gd(DPA)_3]^{3-}$ were determined as the difference in paramagnetic and diamagnetic relaxation rates, where paramagnetic relaxation rates were measured in the presence of $[Gd(DPA)_3]^{3-}$. The diamagnetic relaxation rates were measured at a peptide concentration of 0.3 mM without lanthanide complex present. This data set was used as diamagnetic reference for all paramagnetic relaxation data. Diamagnetic ^1H transverse relaxation rates $R^H_{2,dia}$ were obtained by fitting the measured peak intensities of the two-point experiments to a two-parameter exponential equation (Ferretti and Weiss 1989). Transverse PREs induced by Gd(DTPA-BMA) were measured as for $[Gd(DPA)_3]^{3-}$.

Diamagnetic longitudinal ^1H relaxation rates $R^H_{1,dia}$ were measured by inversion-recovery-^{15}N-HSQC spectra using

relaxation delays of 3 ms, 1 s, and 5 s and an inter-scan recovery delay of 5 s. The measured peak intensities were fitted to a two-parameter exponential equation (Ferretti and Weiss 1989).

Transverse ^{15}N relaxation rates R_2^N were determined by fitting a series of measured peak intensities from ^{15}N-HSQC-type spectra (Farrow et al. 1994) recorded with delays $T = 17.3$, 34.6, 51.8, 69.1, 86.4, 103.7, 121.0, and 138.2 ms to a two-parameter exponential equation.

PCSs were measured as the difference of the ^{1}H chemical shifts observed in the ^{15}N-HSQC spectrum measured in the presence of paramagnetic $[Ln(DPA)_3]^{3-}$ (Ln = Tm^{3+}, Tb^{3+}, or Yb^{3+}) minus the corresponding chemical shifts measured in the presence of the diamagnetic reference, $[Y(DPA)_3]^{3-}$. Each ^{15}N-HSQC spectrum was recorded at a ^{1}H NMR frequency of 600 MHz using 0.1 mM peptide concentration and $[Ln(DPA)_3]^{3-}$-to-peptide ratios of up to five for $[Tm(DPA_3)]^{3-}$ and $[Tb(DPA_3)]^{3-}$ and up to three in the case of $[Yb(DPA_3)]^{3-}$. PCSs were fitted to the structure of the leucine zipper (O'Shea et al. 1991) using Numbat (Schmitz et al. 2008). Numbat fits $\Delta\chi$ tensors to NMR models by minimizing the difference between experimental PCS and the average PCS computed for all models using a single metal position. By presenting the GCN4 leucine zipper dimer coordinates as the coordinates of two NMR models, this option automatically takes into account the PCSs to identical protons in the two monomers, except that the $\Delta\chi$ tensors need to be scaled two-fold to undo the averaging.

Molecular structures were plotted using Molmol (Koradi et al. 1996).

Results

Binding of $[Ln(DPA)_3]^{3-}$

The lanthanide-DPA complex binds to the peptide with a dissociation constant K_D of about 0.5 mM as measured from chemical shift changes observed in a titration experiment with increasing amounts of $[Yb(DPA)_3]^{3-}$ (Fig. S1). Although the leucine zipper is a dimer with two binding sites for the $[Yb(DPA)_3]^{3-}$ complex, simultaneous population of both sites occurred in less than 15% of the dimers at the maximal concentrations used in the titration experiment, justifying use of a 1:1 binding model for determining the K_D value.

Increasing amounts of $[Gd(DPA)_3]^{3-}$ led to broadening and disappearance of an increasing number of cross-peaks near the N-terminus of the peptide (Fig. 1). Chemical shift changes were limited to the vicinity of the N-terminus and also observed upon titration with diamagnetic $[Y(DPA)_3]^{3-}$ (Fig. S1), in agreement with a specific binding site near the N-terminus of the peptide. No amide proton signal could be observed for Met2 because of too rapid proton exchange with the solvent.

PRE data

Quantitative PRE measurements show by far the largest effects near the N-terminus (Fig. 2). This demonstrates that the two helices of the dimer are oriented parallel rather than antiparallel. To observe PREs close to the N-terminus, a $[Gd(DPA)_3]^{3-}$-to-peptide ratio of 0.02:1 proved adequate, while a ratio of 0.4:1 led to more significant PREs for the entire length of the peptide at the expense of excessive line broadening of the first nine residues. In order to obtain data over the entire length of the peptide at 0.12 mM $[Gd(DPA)_3]^{3-}$, we extrapolated unobservable PREs from PREs measured at the next lower Gd^{3+} concentration, using a scaling factor determined by the average ratio of the PREs of the first few residues observable at both $[Gd(DPA)_3]^{3-}$ concentrations.

The result is shown in Fig. 3a. The PREs decay less steeply than expected for a distance dependence following r^{-6}. Following residue 12, the PREs display maxima and minima along the amino acid sequence with a periodicity of 3 to 4 residues. This suggests that these relaxation rates arise from non-specific PREs rather than from the $[Gd(DPA)_3]^{3-}$ complex bound near the N-terminus. Comparison with the crystal structure of the GCN4 leucine zipper shows that, indeed, the minima and maxima closely correspond to the most solvent protected and most solvent exposed amide protons (Fig. 4).

To verify the contribution from non-specific PREs, we repeated the PRE measurements at a fivefold increased peptide concentration (1.5 mM), while the overall concentration of $[Gd(DPA)_3]^{3-}$ remained the same. As expected for a bulk solvent effect, the PREs of the C-terminal half of the peptide barely changed. The bulk solvent effect is also manifested by enhanced PRE of the C-terminal amide proton which is more highly solvent exposed than the amides of the preceding residues (Fig. 2). In contrast, the increased peptide concentration led to significantly smaller PREs for the N-terminal residues which is readily explained by the smaller fraction of peptide molecules carrying the Gd^{3+} complex specifically bound to the N-terminus.

The overall PRE, PRE^{total}, can be written as the sum of PRE^{bound} and $PRE^{solvent}$, where PRE^{bound} is due to a specifically bound $[Gd(DPA)_3]^{3-}$ complex near the N-terminus, and $PRE^{solvent}$ arises from a non-specific bulk effect including non-specifically associated $[Gd(DPA)_3]^{3-}$. $PRE^{solvent}$ appeared to be independent of peptide concentration, as the PREs of residues far from the N-terminus of the peptide were practically independent of peptide

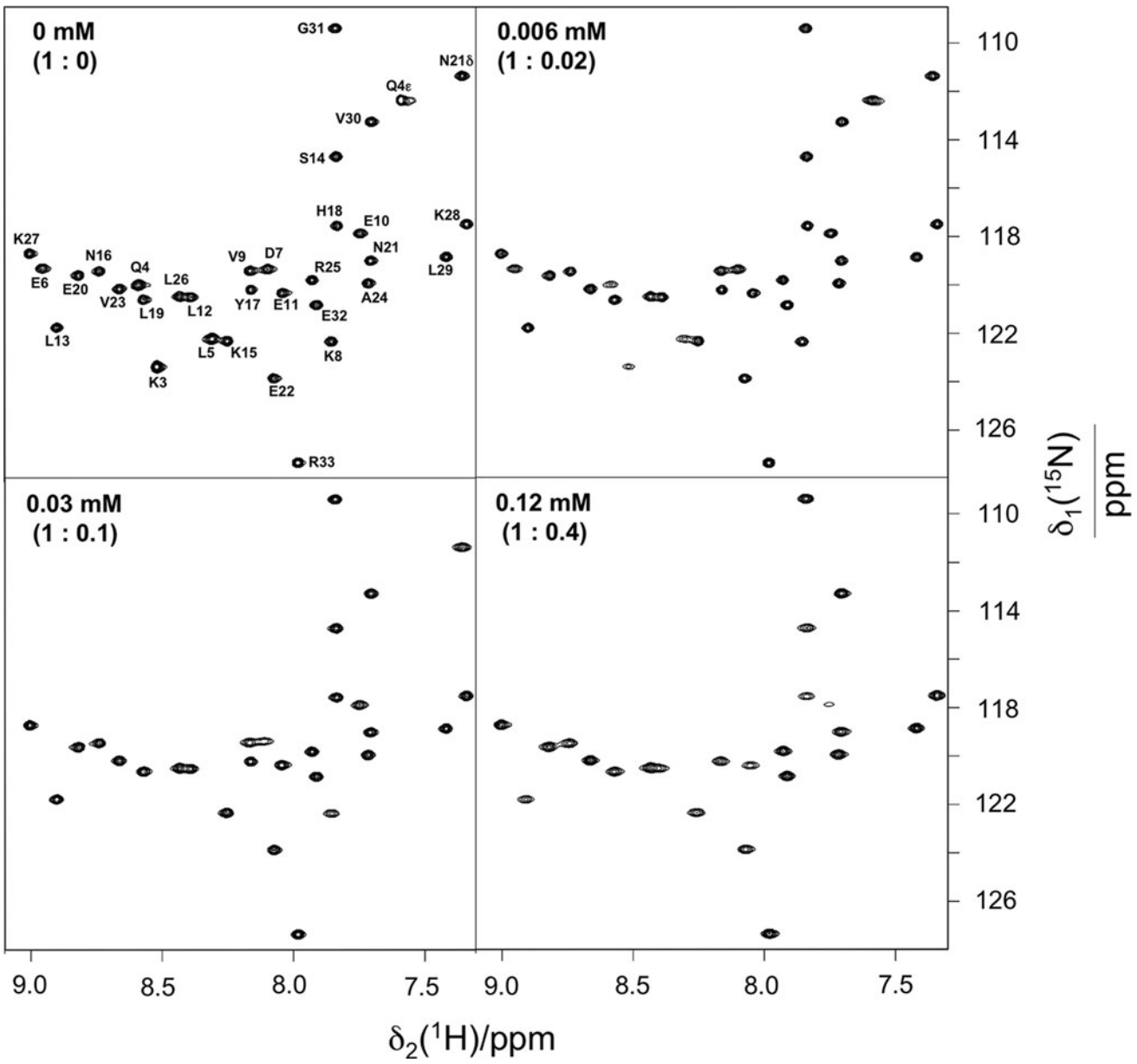

Fig. 1 ^{15}N-HSQC spectra of a 0.3 mM solution of ^{15}N-labeled GCN4 leucine zipper at different concentrations of $[Gd(DPA)_3]^{3-}$

concentration. In contrast, PRE^{bound} is proportional to the population p of peptide with specifically bound $[Gd(DPA)_3]^{3-}$ which can be calculated from the binding constant. Therefore, the following two equations can be used to describe the experiments A and B performed at different peptide concentrations:

$$PRE_A^{total} - PRE_B^{total} = PRE_A^{bound} - PRE_B^{bound} \quad (2)$$

$$PRE_A^{bound}/PRE_B^{bound} = p_A/p_B \quad (3)$$

from which we calculated the PRE^{bound} and $PRE^{solvent}$ values of Fig. 3b. The figure shows that PRE^{bound} effects are pronounced only for the first 14 residues, whereas the PREs of the residues following Ser14 can readily be attributed to the bulk effect.

Unexpectedly, $PRE^{solvent}$ seems to increase towards the N-terminus in concert with PRE^{bound}. The large error ranges associated with the $PRE^{solvent}$ values of the N-terminal residues indicate, however, that the decomposition into PRE^{bound} and $PRE^{solvent}$ is unreliable. It is important to note that the metal position determined from the PRE data is little sensitive with regard to the accuracy of the decomposition. Even if all of the steep increase in $PRE^{solvent}$ towards the N-terminus (residues 3–9 in Fig. 3b) was added to PRE^{bound}, the resulting distance restraints would change by less than 5%.

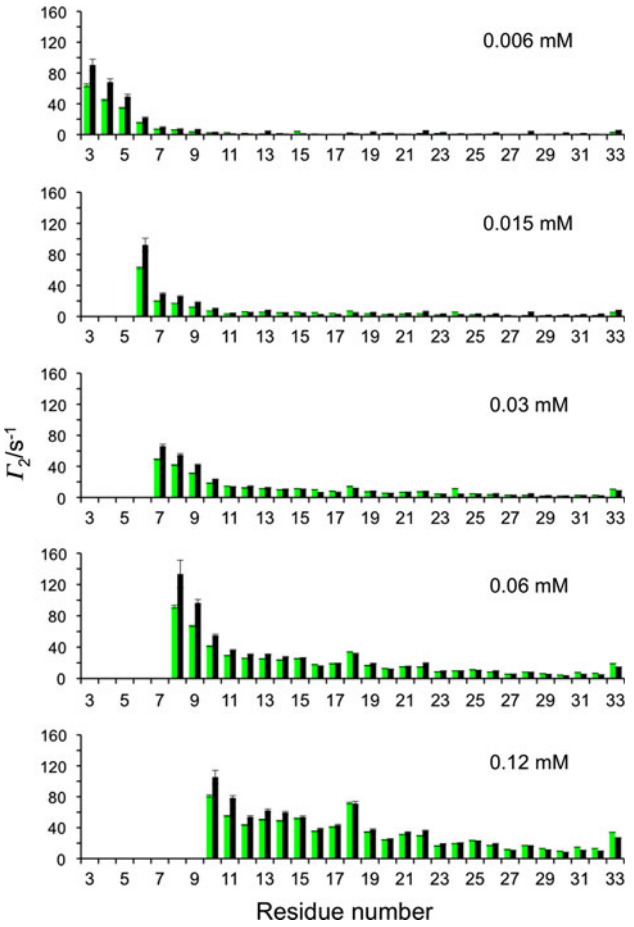

Fig. 2 Amide proton transverse PREs of 0.3 mM (*black*) and 1.5 mM (*green*) solutions of GCN4 leucine zipper at different concentrations of $[Gd(DPA)_3]^{3-}$ as indicated

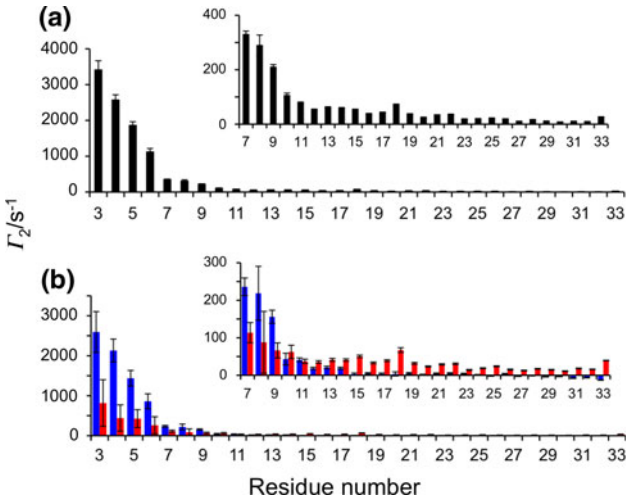

Fig. 3 Overall profiles of transverse ^{1}H PREs of the amide protons of GCN4 leucine zipper. Inserts show the PREs of residues 7–33 on an expanded scale. The plots report PREs for 0.3 mM leucine zipper and 0.12 mM $[Gd(DPA)_3]^{3-}$. Values for residues near the N-terminus were extrapolated from data measured at lower $[Gd(DPA)_3]^{3-}$ concentrations (see main text). **a** Total PREs (Γ_2). **b** Decomposition of the total PREs in **a** into PREs from specifically bound $[Gd(DPA)^3]^{3-}$, PRE^{bound} (*blue*) and from a non-specific bulk solvent effect, $PRE^{solvent}$ (*red*)

Determination of the metal position

The PRE^{bound} data of Fig. 3b (Table S4) were used to fit the position of the metal ion in the dimer by reference to the 3D structure. The crystal structure (PDB code 2ZTA; O'Shea et al. 1991) is not perfectly symmetric while the NMR spectrum displays only a single set of signals, showing that the dimer is symmetric in the time average (Junius et al. 1995; O'Donoghue et al. 1996, Oas et al. 1990, O'Shea et al. 1991). For simplified analysis, we therefore used a symmetrised model for the fits, where monomer 2 of the crystal structure was replaced by monomer 1 following superimposition of monomer 1 on monomer 2 for minimal backbone rmsd. The fits of the PREs used the equation (Kowalewski et al. 1985).

$$\Gamma_2 = 1/2 \sum_{i=1,2} 1/15(\mu_0/4\pi)^2(\mathrm{h}/2\pi)^2\gamma_\mathrm{H}^2(\mathrm{g}\mu_\mathrm{B})^2 \times S(S+1)\mathrm{r}_i^{-6}\left[4\tau + 3\tau/\left(1+\omega_\mathrm{H}^2\tau^2\right)\right] \quad (4)$$

which describes the average paramagnetic enhancement Γ_2 of the transverse relaxation rate of two symmetry-related

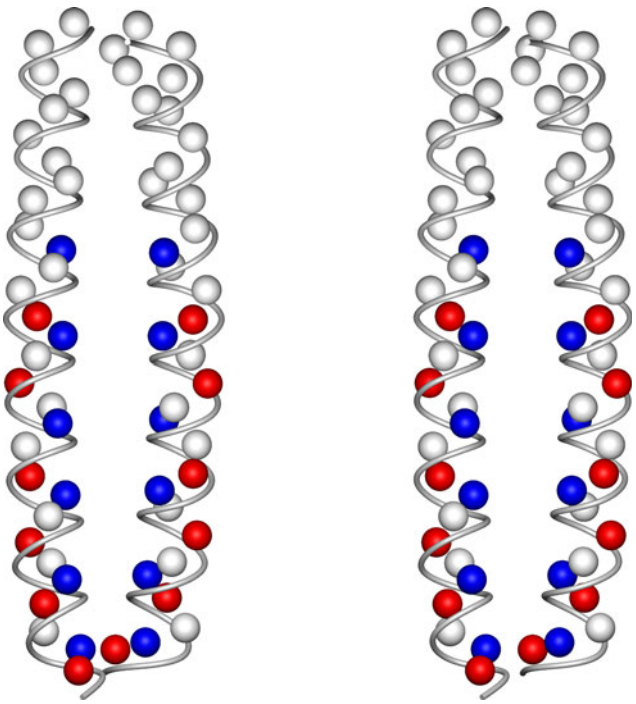

Fig. 4 Stereoview of the GCN4 leucine zipper (crystal structure, PDB code 2ZTA; O'Shea et al. 1991) highlighting the amide protons showing maxima (*red spheres*) and minima (*blue spheres*) of $PRE^{solvent}$ in Fig. 3b. Note that the crystal structure shows no electron density for the C-terminal two residues, i.e. the view ends with Gly31. The N-termini are at the top of the view. The maxima and minima of $PRE^{solvent}$ clearly correlate with solvent exposure

protons in the dimer that are located at distances r_1 and r_2, respectively, from the paramagnetic center. μ_0 is the susceptibility of vacuum, h Planck's constant, γ_H the magnetogyric ratios of the proton, g the Landé factor, μ_B the Bohr magneton, S the electronic spin quantum number, ω_H the Larmor frequency, and τ the effective correlation time given by

$$1/\tau = 1/T_{1e} + 1/\tau_r + 1/\tau_M \quad (5)$$

where T_{1e} is the electronic relaxation time, τ_r the rotational correlation time of the molecule, and τ_M the lifetime of the Gd^{3+}-protein adduct.

Attempts to fit the metal coordinates and the correlation time τ simultaneously identified a metal position that was located too far from the peptide to form any contacts. We therefore reduced the number of variables in the fit by estimating τ as follows. The rotational diffusion of a leucine-zipper is highly anisotropic (Mackay et al. 1996). For a metal binding site near the N-terminus, however, the relevant correlation time τ_r is predominantly determined by the slow molecular tumbling around axes perpendicular to the long axis of the dimer rather than by the faster rotation around the long axis. ^{15}N relaxation is similarly governed by the slow tumbling process, as the amide bonds of the helices are also predominantly aligned with the long axis of the dimer. The transverse relaxation rates $R_2(^{15}N)$ of the amide nitrogens were close to 20 s^{-1} all along the sequence of the peptide (Fig. S4). Assuming an order parameter $S^2 = 0.9$, this translates into $\tau_r = 13.4$ ns. The residence time τ_M of the $[Gd(DPA)_3]^{3-}$ complex near the N-terminus is much longer and therefore can be neglected in Eq. 5. An estimate for τ_M can be obtained by assuming a diffusion limited on-rate $k_{on} = 10^{10}$ $M^{-1}s^{-1}$ which, combined with $K_D = 0.5$ mM, yields an off-rate $k_{off} = K_D \cdot k_{on} = 5 \cdot 10^6$ s^{-1}, the inverse of which corresponds to τ_M.

The electronic relaxation time T_{1e} can be determined from the ratio of transverse and longitudinal PREs (Γ_2/Γ_1) of the amide protons (Pintacuda et al. 2004b). This ratio, measured at 800 MHz, decreased from Lys3, where it was about 430, to about 30 near the C-terminus (Fig. S5). A Γ_2/Γ_1 ratio of 430 translates into an effective correlation time τ of 5 ns. Combined with $\tau_r = 13.4$ ns and a long residence time τ_M of the specifically bound $[Gd(DPA)_3]^{3-}$ complex, $\tau = 5$ ns corresponds to $T_{1e} = 8$ ns (Eq. 5), in good agreement with T_{1e} values determined for different Gd^{3+} complexes by EPR (Benmelouka et al. 2007). It is interesting to note that τ is not very sensitive to the Γ_2/Γ_1 ratio in the regime of large Γ_2/Γ_1 values. For example, a Γ_2/Γ_1 ratio of about 900 would have translated into $\tau = 7.3$ ns.

The metal position was found by minimizing the sum of the squared deviations between experimental and back-calculated transverse PREs of each amide proton using Eq. 4 with $\tau = 5$ ns, $\omega_H = 2\pi$*800 MHz, and $S = 7/2$ for Gd^{3+}:

$$\Gamma_2/[s^{-1}] = 5.1 \cdot 10^9 \, 1/2 \sum_{i=1,2} (r_i/[Å])^{-6} \quad (6)$$

Equation 6 is valid irrespective of whether one or two $[Gd(DPA)_3]^{3-}$ complexes are bound to the dimer, as either binding site leads to relaxation enhancements of all nuclear spins in the dimer and fast chemical exchange between the two sites ensures that all nuclear spins experience an average relaxation rate. Under our conditions (0.3 mM peptide, 0.12 mM $[Gd(DPA)_3]^{3-}$, $K_D = 0.5$ mM), only one in 7.5 binding sites was occupied by the Gd-DPA complex. Therefore, we scaled the experimentally measured PREs 7.5 fold before fitting. (Using the K_D values determined from the signals of Lys3 and Leu5 (0.7 and 0.38 mM, respectively, Fig. S1) would have changed this scaling factor relatively little, namely to 9.0 and 6.3, respectively.)

Figure 5 shows the two symmetry-related metal ion positions obtained from the fit. The binding site of the $[Gd(DPA)_3]^{3-}$ complex is between the side chain of Met2 of one monomer and the N-terminus and the side chain of Lys3 of the other monomer. The symmetry-related metal positions are separated by about 13 Å. Under the conditions used, however, each $[Gd(DPA)_3]^{3-}$ binding site was populated to less than 15% and dimers with two bound $[Gd(DPA)_3]^{3-}$ complexes would have occurred with a probability of less than 2%.

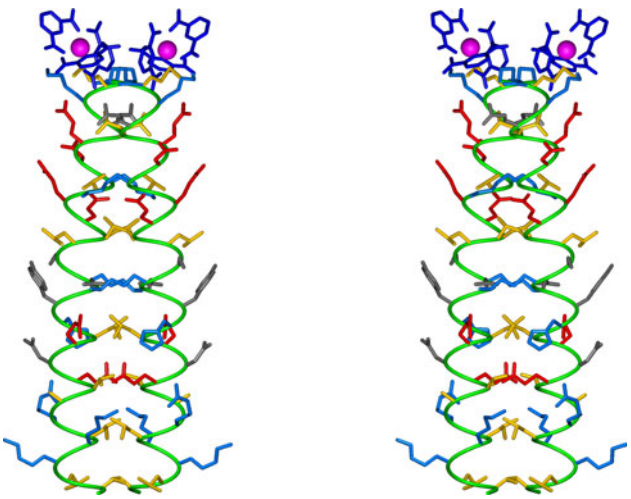

Fig. 5 Stereoview of the GCN4 leucine zipper with bound $[Gd(DPA)_3]^{3-}$ complexes. The metal positions (magenta balls) were determined using the PRE^{bound} values of Table S4. The amino acid side chains are shown in a heavy atom representation in the following colors: blue (Arg, His, Lys), red (Asp, Glu), grey (Asn, Gln, Ser, Tyr), yellow (Ala, Leu, Met, Val). The orientation of the DPA molecules of the $[Gd(DPA)_3]^{3-}$ complexes has not be determined experimentally

Assessment of the dimer structure by PCSs

The metal coordinates obtained from the PRE data were used to assist the fitting of PCSs detected with the corresponding DPA complexes of Tm^{3+}, Tb^{3+}, and Yb^{3+} (Table 1). As only a small number of PCSs could be detected for each metal ion (Table S5), prior knowledge of the metal coordinates led to an important reduction in the number of parameters. As expected, the PCSs observed with Tm-, Tb- and Yb-DPA complexes were in better agreement with the structure of dimeric leucine zipper than with a single monomeric helix of the dimer (Fig. 6).

To probe the information content of the PCSs about the dimer interface, we produced 35 additional models, where each helix was rotated around its axis (defined by the 10 amino terminal residues) in 10 degree increments. The symmetry of the dimer was maintained by rotating the monomers in the opposite sense. In addition, the metal position was retained by treating the complex of helix and $[Gd(DPA)_3]^{3-}$ as a rigid unit. Fig. 7 shows the sum of the squared deviations of the best fits obtained for each of the 36 models versus the rotation angle. For Yb^{3+} and Tm^{3+}, the unrotated dimer model clearly produced the best fit. The Tb^{3+} data suggested a better fit with a model rotated by 30°, but as the PRE effect associated with Tb^{3+} broadened the amide proton signals of residues 3–5 beyond detection, the fit of the $\Delta\chi$ tensor of Tb^{3+} was less reliable. This illustrates the power of PCSs to define the dimer interface in solution but also the importance of probing the immediate environment of the metal ion.

Without prior knowledge of the metal position, even discrimination between monomer and dimer models by PCSs would have been ambiguous. In fact, using exclusively the PCSs of Tb^{3+}, Tm^{3+}, and Yb^{3+} in a multiparameter fit to the dimer structure yielded a metal ion position 4.5 Å from the position determined by PREs. Even including the proportionality factor in Eq. 6 as an additional fitting parameter shifted the metal position by less than 2.4 Å (data not shown), illustrating the robustness with which the metal position can be determined from short-range PREs.

Table 1 $\Delta\chi$ tensor parameters of paramagnetic $[Ln(DPA)_3]^{3-}$ complexes bound to dimeric leucine zipper[a]

Ln^{3+}	$\Delta\chi_{ax}$ (10^{-32} m^3)	$\Delta\chi_{rh}$ (10^{-32} m^3)
Tb^{3+} [a]	−31.1	−7.1
Tm^{3+} [a]	18.9	11.8
Yb^{3+} [b]	8.7	4.6

[a] The tensor parameters obtained by Numbat (Schmitz et al. 2008) were scaled 4.2-fold to relate to the 1:1 complex of $[Ln(DPA)_3]^{3-}$ to leucine zipper monomer. This accounts for averaging in Numbat (see Materials and Methods) and the fact that only 1 in 2.1 peptide molecules are associated with a $[Ln(DPA)_3]^{3-}$ complex at peptide and $[Ln(DPA)_3]^{3-}$ concentrations of 0.1 and 0.5 mM, respectively

[b] The tensor parameters were scaled 5.8-fold to account for peptide and $[Yb(DPA)_3]^{3-}$ concentrations of 0.1 and 0.3 mM, respectively (only one in 2.9 peptide molecules were associated with a $[Yb(DPA)_3]^{3-}$ complex)

Comparison of $[Gd(DPA)_3]^{3-}$ with Gd(DTPA-BMA) as an indicator of solvent accessibility

The bulk solvent effect was evident in unaltered PRE effects, when data were recorded at fivefold increased peptide concentrations (Fig. 2). The lifetime τ_M of the intermolecular adducts contributing to the bulk solvent effect is short. The Γ_2/Γ_1 ratio of 35 observed for the amide of Val30 with $[Gd(DPA)_3]^{3-}$ (Fig. S5) indicates an effective correlation time τ_c of 1.4 ns which, using Eq. 5 with $T_{1e} = 8$ ns and $\tau_r = 13.4$ ns yields $\tau_M = 2$ ns. This is longer than $\tau_M = 0.6$ ns reported previously for the uncharged Gd(DTPA-BMA) complex (Pintacuda and Otting 2002). τ_M increases to 2.3 ns if one assumes $\tau_r = 6.7$ ns to account for the possibility that the effective rotational correlation time of the bulk solvent PRE is predominantly governed by rotation along the long axis of the dimer. In any case, the DPA complex appears to be more "sticky" than the DTPA-BMA complex. This is also evidenced by the PRE maximum observed for the amide proton of His18 (Fig. 8) which can be explained by a preference of the DPA complex for positively charged amino acid side chains. Interaction of the negative charge of the DPA complex with the helix dipole moment may also explain the gradual increase in the bulk solvent contribution to the PRE towards the N-terminus, as favourable charge-charge interaction would be expected to lead to longer lifetimes of non-specific intermolecular adducts. This interpretation is supported by Γ_2 measurements performed with GCN4 leucine zipper and the uncharged complex Gd(DTPA-BMA) which showed much more uniform PREs along the helix (Fig. 8). In addition, the PRE effects observed with 2 mM Gd(DTPA-BMA) were always smaller than those achieved with 0.12 mM $[Gd(DPA)_3]^{3-}$, indicating that $[Gd(DPA)_3]^{3-}$ associates more readily with protein surfaces.

Discussion

Accuracy of the metal position determined by PREs from $[Gd(DPA)_3]^{3-}$

The non-covalent complex between $[Gd(DPA)_3]^{3-}$ and the GCN4 leucine zipper allows determination of the metal binding site with unprecedented accuracy. Using PCSs only to find the metal position in a known protein structure

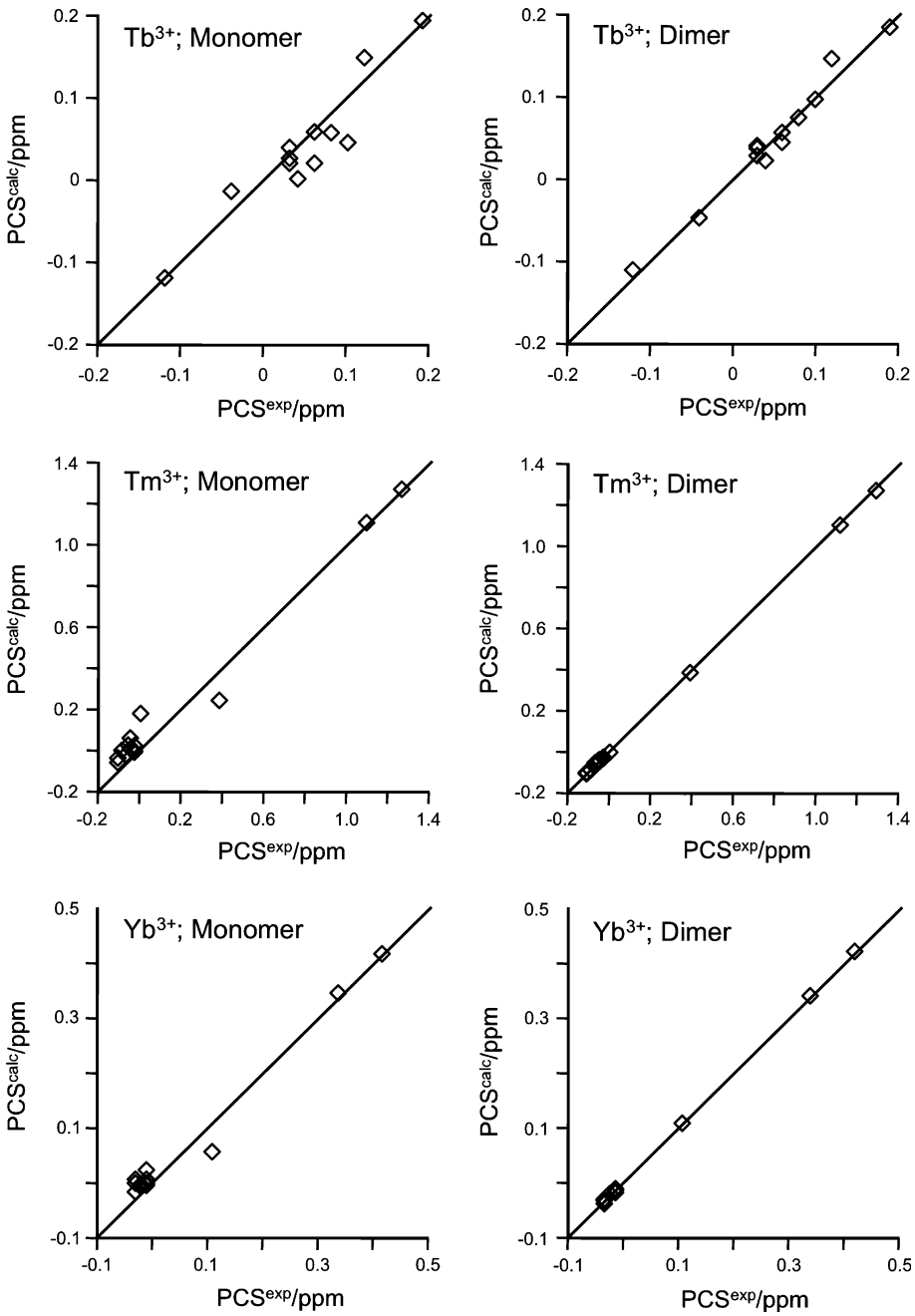

Fig. 6 Back-calculated versus experimental pseudocontact shifts of backbone amide protons of the GCN4 leucine zipper. The experimental PCS data were recorded at a molar ratio of $[Ln(DPA)_3]^{3-}$ to protein of 5:1 in the cases of the Tm^{3+} and Tb^{3+} complexes and at a molar ratio of 3:1 in the case of the Yb^{3+} complex (Table S5). Fits to the dimer structure are clearly better than fits to a single helix of the leucine zipper (monomer). All fits used the metal ion position determined from the PRE data generated with $[Gd(DPA)_3]^{3-}$

usually produces much less stable results for a number of reasons. (1) PCS data require an eight-parameter fit, including the x, y and z-coordinates of the metal position, the axial and rhombic components of the $\Delta\chi$ tensor and three angles describing its orientation with respect to the protein structure. In contrast, PRE data can be directly converted into distance restraints and only the metal coordinates need to be fitted. (2) Metal ions generating large PCSs invariably also produce large PREs. Therefore, choosing a strongly paramagnetic metal ion tends to yield PCSs for a greater number of nuclei, but PCSs of nuclei close to the metal ion are difficult to observe. Choosing a weakly paramagnetic metal ion renders PCSs of nuclei near the metal ion observable, but the number of nuclei with significant PCSs is limited. More accurate fits can be obtained by using PCSs from strongly and weakly paramagnetic metal ions simultaneously (Man et al. 2010), although this also increases the number of parameters that need to be fitted. (3) The much steeper distance dependence of PREs versus PCSs (i.e. r^{-6} versus r^{-3}) renders distance measurements by PREs less sensitive to experimental error.

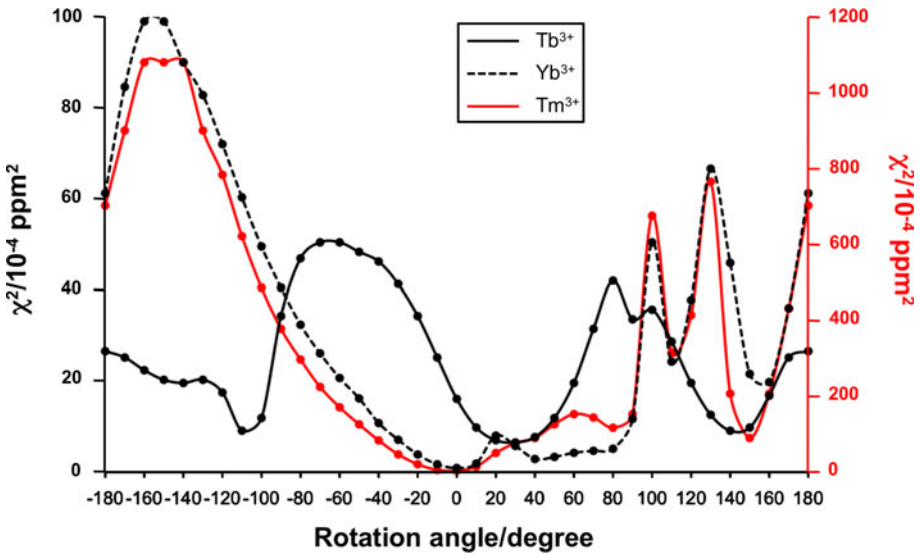

Fig. 7 Sum of the squared deviations, χ^2, of the best fits of the amide proton PCSs observed for $[Ln(DPA)_3]^{3-}$ complexes with Tb^{3+} (black solid line), Yb^{3+} (*black dashed line*) and Tm^{3+} (*red solid line*). The χ^2 values are plotted against the rotation angle of the helices (see main text)

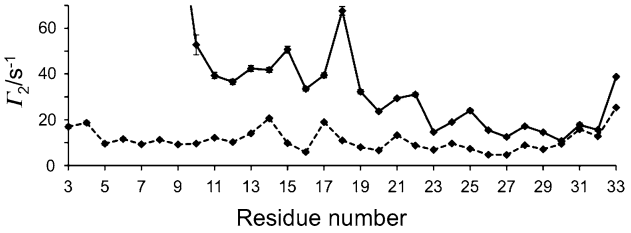

Fig. 8 Amide proton transverse PREs of an 0.3 mM solution of GCN4 leucine zipper with 2 mM Gd(DTPA-BMA) (*dashed line*) and 0.12 mM $[Gd(DPA)_3]^{3-}$ (*solid line*) versus amino acid sequence

As Mn^{2+}, Gd^{3+}, and nitroxide radicals all generate pronounced PREs, it is usually difficult to observe signals of nuclei close to these paramagnetic centers, making it correspondingly difficult to pinpoint the metal position. Furthermore, most available paramagnetic tags attach the paramagnetic center to the protein via flexible linkers (Su and Otting 2010) leading to intrinsically ambiguous metal positions. The $[Gd(DPA)_3]^{3-}$ complex solves both problems, as the PREs can be scaled down by using smaller quantities of the $[Gd(DPA)_3]^{3-}$ complex and specific binding to the protein with good affinity is likely to involve only a single well-defined low-energy binding site. Partial saturation of conventional, covalently attached metal tags with Gd^{3+} is not a viable alternative as all known tags display slow chemical exchange between bound and free metal ion.

The conversion of PREs into distance restraints depends on the population of the binding site with the gadolinium complex, the contribution of the specific versus bulk solvent effect, and the effective correlation time. In principle, all these parameters can be taken into account by including the proportionality factor between the PRE and r_i (Eq. 6) in the fit as a fitting parameter. In the case of the GCN4 leucine zipper, however, this resulted in a less accurate metal position with unrealistically few contacts between the Gd^{3+} complex and the peptide. Fortunately, the correct proportionality factor can be estimated with acceptable accuracy without a host of additional measurements.

Due to the steep distance dependence of PREs, even a twofold error in the population of bound peptide, effective correlation time, or PRE^{bound} changes the distance restraints by less than 13%. Therefore, the metal position could still be determined with high accuracy if no attempt was made to separate PRE^{bound} from PRE^{total} (Fig. 3b). It is beneficial that the metal position is governed by the shortest distance restraints, because the fit which minimizes the sum of the squared deviations between experimental and back-calculated PREs is governed by the large PREs of the nuclear spins nearest to the paramagnetic center.

The elongated shape of the leucine zipper renders description by a single rotational correlation time inaccurate. In the case of a different, somewhat longer leucine zipper, the correlation time for rotations along the long axis of the dimer was found to be about twofold shorter than for motions along a perpendicular axis (Mackay et al. 1996). The influence of the rotational correlation time on the effective correlation time is, however, reduced when it is longer than the electronic relaxation time or the exchange lifetime (Eq. 5). The present work determined an electronic relaxation time T_{1e} of 8 ns for the $[Gd(DPA)_3]^{3-}$ complex.

A simplified protocol would estimate the effective correlation time by using the T_{1e} value determined here and estimating the rotational correlation time of the protein from its molecular weight. In the case of the GCN4 leucine zipper, adequate PRE values for fitting the metal position would have been obtained by subtracting a rate of 100 s^{-1} from every PRE^{total} value of Fig. 3a and ignoring any resulting negative PRE values. The fraction of protein molecules with bound DPA complex can readily be

measured by titration with a $[Ln(DPA)_3]^{3-}$ complex that amplifies the chemical shift changes by inducing PCSs. With these parameters, the metal position can be determined from two-point relaxation measurements in the presence and absence of $[Gd(DPA)_3]^{3-}$, using a single protein concentration and a single $[Gd(DPA)_3]^{3-}$ concentration which must be sufficiently low to allow measurement of PRE effects in the vicinity of the paramagnetic center. The optimal concentrations can readily be estimated from the binding affinity.

Restraints for analysis of quaternary structure

Using the $[Gd(DPA)_3]^{3-}$ complex alone to elucidate the structure of the GCN4 homodimer would be much more difficult to achieve than by the use of PCSs because, due to the steep distance dependence of PRE effects, the fit of the metal coordinates is strongly dominated by the shorter one of the distances to the two symmetry-related protons. Therefore, short-range PREs and long-range PCSs present highly complementary structure restraints.

In general, determination of the quaternary structure would be best performed by a simultaneous fit of PREs and PCSs during modelling, including symmetry constraints if necessary. Such a protocol would be particularly important, if the metal ion is positioned so close to the dimer interface that the contribution of the symmetry related spin to the average PRE can no longer be neglected.

Requirements of binding kinetics

So long as the presence of a $[Ln(DPA)_3]^{3-}$ complex bound to one of the monomers of the dimer does not affect binding of a second $[Ln(DPA)_3]^{3-}$ complex to the other monomer, the fast exchange of the lanthanide-DPA complex between monomers ensures that the relative magnitudes of PREs and PCSs observed for different peptide resonances are the same for the 1:2 and 2:2 complexes of $[Ln(DPA)_3]^{3-}$ to peptide (monomer). This greatly facilitates data analysis.

Adequate averaging of the relaxation rates of peptide molecules with and without bound paramagnetic complex requires that averaging between the free and bound peptide molecules is faster than the fastest relaxation rate. For a typical diffusion limited on-rate $k_{on} = 10^{10}\ M^{-1}s^{-1}$ and a dissociation constant $K_D = 1\ \mu M$, the off-rate $k_{off} = K_D \cdot k_{on} = 10^4\ s^{-1}$ would be faster than 4,000 s^{-1} which was the fastest relaxation rate determined for the GCN4 leucine zipper (Fig. 3). Therefore, weakly binding paramagnetic complexes readily fulfill the condition of fast exchange. Complexes binding with $K_D < 1\ \mu M$ are usually in the slow exchange regime which would easily be detected in a titration experiment.

Conclusion

The combination of PREs and PCSs induced by non-covalently binding $[Ln(DPA)_3]^{3-}$ complexes presents outstanding opportunities for the analysis of protein structure and protein–ligand interactions. Although many proteins bind $[Ln(DPA)_3]^{3-}$ complexes with high site-specificity (Su et al. 2009), the presence or absence of natural binding sites cannot always be predicted. In the case of the GCN4 leucine-zipper, specific binding of the negatively charged lanthanide-DPA complex near the N-terminus is probably supported by the helix dipole moment. For proteins devoid of natural $[Ln(DPA)_3]^{3-}$ binding sites, a specific binding site can readily be created by site-directed mutagenesis (H. Yagi, unpublished results). Combined with the use of the $[Gd(DPA)_3]^{3-}$ complex to determine the metal position accurately, this opens the door to applications of PCSs induced by $[Ln(DPA)_3]^{3-}$ complexes in challenging structure analysis projects. It is particularly encouraging that the present analysis of the GCN4 homodimer could be performed using exclusively data from well-resolved ^{15}N-^{1}H correlation spectra.

Acknowledgments Financial support by the Australian Research Council is gratefully acknowledged.

References

Arnesano F, Banci L, Piccioli M (2005) NMR structures of paramagnetic metalloproteins. Quart Rev Biophys 38:167–219

Baker RT, Catanzariti AM, Karunasekara Y, Soboleva TA, Sharwood R, Whitney S, Board PG (2005) Using deubiquitylating enzymes as research tools. Methods Enzymol 398:540–554

Balayssac S, Bertini I, Bhaumik A, Lelli M, Luchinat C (2008) Paramagnetic shifts in solid-state NMR of proteins to elicit structural information. Proc Natl Acad Sci 105:17284–17289

Benmelouka M, Borel A, Moriggi L, Helm L, Merbach AE (2007) Design of Gd(III)-based magnetic resonance imaging contrast agents: static and transient zero-field splitting contributions to the electronic relaxation and their impact on relaxivity. J Phys Chem B 111:832–840

Bertini I, Luchinat C, Parigi G, Pierattelli R (2008) NMR spectroscopy of paramagnetic metalloproteins. Dalton Trans 2008:3782–3790

Bloembergen N, Morgan LO (1961) Proton relaxation times in paramagnetic solutions. Effects of electron spin relaxation. J Chem Phys 34:842–850

Clore GM, Iwahara J (2009) Theory, practice, and applications of paramagnetic relaxation enhancement for the characterization of transient low-population states of biological macromolecules and their complexes. Chem Rev 109:4108–4139

Farrow NE, Muhandiram R, Singer AU, Pascal SM, Kay CM, Gish G, Shoelson SE, Pawson T, Forman-Kay JD, Kay LE (1994) Backbone dynamics of a free and a phosphopeptide-complexed Src homology 2 domain studied by ^{15}N NMR relaxation. Biochemistry 33:5984–6003

Ferretti JA, Weiss GH (1989) One-dimensional nuclear Overhauser effects and peak intensity measurements. Meth Enzymol 176: 3–11

Guéron M (1975) Nuclear relaxation in macromolecules by paramagnetic ions–novel mechanism. J Magn Reson 19:249–273

Iwahara J, Tang C, Clore GM (2007) Practical aspects of ^{1}H transverse paramagnetic relaxation enhancement measurements on macromolecules. J Magn Reson 184:185–195

Junius FK, Mackay JP, Bubb WA, Jensen SA, Weiss AS, King GF (1995) Nuclear magnetic resonance characterization of the Jun leucine-zipper domain–unusual properties of coiled-coil interfacial polar residues. Biochemistry 34:6164–6174

Koradi R, Billeter M, Wüthrich K (1996) MOLMOL: a program for display and analysis of macromolecular structures. J Mol Graphics 14:51–55

Kowalewski J, Nordenskiöld L, Benetis N, Westlund PO (1985) Theory of nuclear-spin relaxation in paramagnetic systems in solution. Prog NMR Spectr 17:141–185

Mackay JP, Shaw GL, King GF (1996) Backbone dynamics of the c-Jun leucine zipper: ^{15}N NMR relaxation studies. Biochemistry 35:4867–4877

Man B, Su XC, Liang H, Simonsen S, Huber T, Messerle BA, Otting G (2010) 3-Mercapto-2,6-pyridinedicarboxylic acid: a small lanthanide-binding tag for protein studies by NMR spectroscopy. Chem Eur J 16:3827–3832

Matousek WM, Ciani B, Fitch CA, Garcia-Moreno B, Kammerer RA, Alexandrescu AT (2007) Electrostatic contributions to the stability of the GCN4 leucine zipper structure. J Mol Biol 374:206–219

O'Donoghue SI, King GF, Nilges M (1996) Calculation of symmetric multimer structures from NMR data using a priori knowledge of the monomer structure, co-monomer restraints, and interface mapping: the case of leucine zippers. J Biomol NMR 8:193–206

O'Shea EK, Rutkowski R, Kim PS (1989) Evidence that the leucine zipper is a coiled coil. Science 243:538–542

O'Shea EK, Klemm JD, Kim PS, Alber T (1991) X-ray structure of the GCN4 leucine zipper, a 2-stranded, parallel coiled coil. Science 254:539–544

Oas TG, McIntosh LP, O'Shea EK, Dahlquist FW, Kim PS (1990) Secondary structure of a leucine zipper determined by nuclear magnetic resonance spectroscopy. Biochemistry 29:2891–2894

Otting G (2008) Prospects for lanthanides in structural biology by NMR. J Biomol NMR 42:1–9

Pintacuda G, Otting G (2002) Identification of protein surfaces by NMR measurements with a paramagnetic Gd(III) chelate. J Am Chem Soc 124:372–373

Pintacuda G, Kaikkonen A, Otting G (2004a) Modulation of the distance dependence of paramagnetic relaxation enhancements by CSAxDSA cross-correlation. J Magn Reson 171:233–243

Pintacuda G, Moshref A, Leonchiks A, Sharipo A, Otting G (2004b) Site-specific labelling with a metal chelator for protein-structure refinement. J Biomol NMR 29:351–361

Pintacuda G, John M, Su XC, Otting G (2007) NMR structure determination of protein-ligand complexes by lanthanide labeling. Acc Chem Res 40:206–212

Schmitz C, Stanton-Cook MJ, Su XC, Otting G, Huber T (2008) Numbat: an interactive software tool for fitting $\Delta\chi$-tensors to molecular coordinates using pseudocontact shifts. J Biomol NMR 41:179–189

Solomon I (1955) Relaxation processes in a system of two spins. Phys Rev 99:559–565

Su XC, Otting G (2010) Paramagnetic labelling of proteins and oligonucleotides for NMR. J Biomol NMR 46:101–112

Su XC, Liang H, Loscha KV, Otting G (2009) $[Ln(DPA)_3]^{3-}$ is a convenient paramagnetic shift reagent for protein NMR studies. J Am Chem Soc 131:10352–10353

Ubbink M (2009) The courtship of proteins: understanding the encounter complex. FEBS Lett 583:1060–1066

Vega AJ, Fiat D (1976) Nuclear relaxation processes of paramagnetic complexes. The slow-motion case. Mol Phys 31:347–355

Vold RL, Waugh JS, Klein MP, Phelps DE (1968) Measurement of spin relaxation in complex systems. J Chem Phys 48:3831–3832

Zweckstetter M, Schnell JR, Chou JJ (2005) Determination of the packing mode of the coiled-coil domain of cGMP-dependent protein kinase Iα in solution using charge-predicted dipolar couplings. J Am Chem Soc 127:11918–11919